

D. B. Hill · M. J. Plaza · K. Bonin · G. Holzwarth

Fast vesicle transport in PC12 neurites: velocities and forces

Received: 25 September 2003 / Revised: 26 February 2004/Accepted: 8 March 2004 / Published online: 8 April 2004
© EBSA 2004

Abstract Although the mechanical behavior of single-motor protein molecules such as kinesin has been carefully studied in buffer, the mechanical behavior of motor-driven vesicles in cells is much less understood. We have tracked single vesicles in neurites of PC12 cells with a spatial precision of ± 30 nm and a time resolution of 120 ms. Because the neurites are thin, long, straight, and attached to the surface of planar cover glasses, the velocity of individual vesicles could be measured for times as long as 15 s and distances as long as 15 μ m. The velocity of anterograde vesicles was in most cases constant for periods of 1–2 s, then changed in a step-like fashion to a new constant velocity. The viscoelastic modulus felt by the vesicles within live PC12 cells was determined from the Brownian motion, using Mason's generalization of the Stokes–Einstein equation. From Stokes' law, the drag force at the smallest sustained velocity was 4.2 ± 0.6 pN for vesicles of radius 0.30–0.40 μ m, about half the maximum force which conventional kinesin can develop during bead assays in buffer. We interpret the observed velocity steps as changes of ± 1 or occasionally ± 2 in the number of active motor proteins dragging that vesicle along a microtubule. Assuming that the motor is conventional kinesin, which hydrolyzes one ATP per 8 nm step along the microtubule, the motor protein efficiency in PC12 neurites is approximately 35%.

Keywords Motor-driven vesicles · Neurites · PC12 cells · Vesicle velocity

Introduction

It has long been noted that fast transport of vesicles in cells occurs in a jerky and interrupted manner termed saltatory motion (Brady et al. 1982; Freed and Lebowitz 1970; Rebuhn 1967). In mammalian neurons, transport velocities in the range 70–300 μ m/day (0.8–3.5 μ m/s) are classified as “fast” (Grafstein and Forman 1980). Fast transport over long distances, as in axons, is carried out primarily by motor proteins of the kinesin and dynein families, using microtubules as a spatially fixed vectorial track over the time-scale of the motion (Goldstein and Yang 2000; Howard 2001; Schliwa 2003).

The mechanochemistry of single kinesin molecules has been studied with great success by using an optical trap or glass fiber as a force sensor with piconewton sensitivity (Meyhoefer and Howard 1995; Svoboda et al. 1993; Vale et al. 1996; Visscher et al. 1999). These experiments show that a single conventional kinesin molecule can move an attached bead at 800 nm/s when the opposing force is less than 1 pN. When the opposing force increases from 1 to 7.5 pN, the velocity decreases to zero. In microtubule gliding assays, kinesin is adsorbed onto a glass surface and the bound microtubule moves through the medium. Drag forces on the microtubule, or a fine glass needle restraining the microtubule, thus become the load on the motor. By measuring the deflection of the needle, Meyhoefer and Howard (1995) found that the limiting force for single kinesin motors is 5.4 ± 1.0 pN. In gliding assays at low load (in buffer), the velocity of the microtubule load is independent of the number density of motors (Howard et al. 1989). However, in gliding assays at higher loads (in a viscous medium) the velocity increases with increasing kinesin density (Hunt et al. 1994). The stall force extracted from these observations increases from 4.2 pN with one kinesin to 16 pN as the number of attached kinesins increases (Hunt et al. 1994).

The application of these ingenious single-motor observations and concepts to vesicle transport in cells

D. B. Hill · M. J. Plaza · K. Bonin · G. Holzwarth (✉)
Department of Physics, Wake Forest University,
Winston-Salem, NC 27109, USA
E-mail: gholz@wfu.edu
Tel.: +1-336-7585533
Fax: +1-336-7586142

Present address: D. B. Hill
Department of Physics,
University of North Carolina,
Chapel Hill, NC 27599, USA

needs to be done carefully. One reason is that the load on the motor is about three orders of magnitude larger in the cell than in most in vitro experiments. A second reason is that no definitive method currently exists for determining the number of active motors pulling a vesicle in a live cell, although electron microscopy (EM) images of fixed cells suggest that the number of attached motors is only 2–3 (Ashkin et al. 1990; Hirokawa 1998). In addition, vesicles have a range of sizes, shapes, and surface compositions, so that the drag forces for different vesicles are not expected to be identical, even if they are moving at the same speed. Finally, the drag force on a moving vesicle may change upon encountering a microtubule-associated protein such as tau, or when it encounters a cytoskeletal obstacle.

A question of particular concern is whether the velocity of a kinesin-driven vesicle in a cell is independent of the number of active motors. On the one hand, careful measurements of single-motor operation in an optical trap show that the velocity decreases almost linearly with load in the 1–10 pN range (Fig. 1) (Kojima et al. 1997; Meyhoefer and Howard 1995; Visscher et al. 1999). This suggests that vesicle speed and the stall force should *increase* with an increasing number of motors, because the load would be divided between the motors; see Fig. 1. On the other hand, microtubule gliding assays in buffer suggest that the velocity should be independent of the number of motors at low load, but dependent on the number of motors at higher load. The dilemma can be resolved if one recognizes the force domain applicable to a particular experiment. For gliding assays in buffer

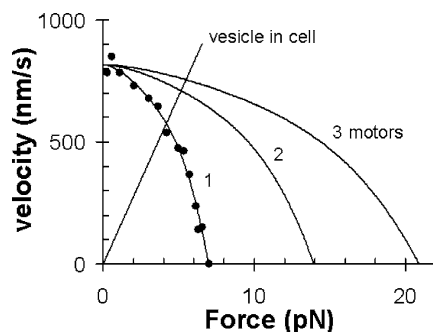


Fig. 1 The velocity of a vesicle or bead pulled by conventional kinesin as a function of retarding force. The *circles* are experimental data for a single kinesin motor attached to a bead in an optical trap (Schnitzer et al. 2000). The curves for 2 and 3 kinesins are constructed from the bead-assay curve by assuming that the load is shared among the motors. The *straight line* through the origin corresponds to Stokes' law for a sphere of radius $0.4 \mu\text{m}$ in a medium with $\eta = 1.1 \text{ Pa s}$. The retarding force in microtubule gliding assays is small: $0 < F < 0.1 \text{ pN}$. In this regime, no change in velocity with the number of motors is expected. Note that the maximum velocity of vesicles in cells is usually larger than the bead-assay maximum shown in the figure. Typical cellular values of V_{max} in neurons are 3500 nm/s (Grafstein and Forman 1980), 4500 nm/s (Kaether et al. 2000), and 5000 nm/s (Brady et al. 1982). Measurements of F_{max} in cells are sparse: Weischaus and Block measured stall forces of 1–5 pN for lipid droplets in *Drosophila* embryos (Welte et al. 1998)

the force is only 0.027 pN (Gibbons et al. 2001); in this force regime (Fig. 1), adding more motors is not expected to change the speed of the vesicle. However, if the load is 1–20 pN, the velocity should increase with an increasing number of motors (Fig. 1 and Hunt et al. 1994).

The force required to stop a vesicle or mitochondrion in live cells has been measured by optical trap techniques in two biological systems. In *Reticulomyxa*, small mitochondria were prevented from moving with a 3 pN opposing force (Ashkin et al. 1990). In *Drosophila* embryos, endogenous lipid droplets were stopped by opposing forces in the range $1.1\text{--}5.5 \text{ pN}$ (Welte et al. 1998).

The understanding of fast axonal transport was notably advanced in 1982 when Allen et al. (1982) showed that small vesicles could be tracked in squid giant axon by background-subtracted DIC microscopy. Particles with apparent radii in the range $50\text{--}100 \text{ nm}$ moved at $2.5 \mu\text{m/s}$, whereas larger particles with $400\text{--}2500 \text{ nm}$ radius had an average velocity of only $1 \mu\text{m/s}$. It was noted that particles of intermediate size sometimes moved at one velocity, stopped momentarily, then resumed motion at a different velocity.

In this paper, we have studied the problem of vesicle transport in live cells with the benefit of improved technology and the insights afforded by the identification and characterization of motor molecules. We have measured the velocity of single vesicles in neurites of PC12 cells, which are widely used as a model system for neuronal development (Greene et al. 1998). Upon treatment with neuronal growth factor, PC12 cells extend long, straight, thin neurites that adhere to a microscope coverslip. This means that long stretches of an intact neurite can be in focus at one time. Since vesicles are confined to the neurite, they can be tracked over long distances (and thus long times) without going out of focus. DIC microscopy has the advantage that it does not damage cells. In the past, on-line background-subtraction was done with an analog camera and 8-bit computation. We use a 12-bit digital camera and 12-bit processing to do on-line background subtraction. This improves the number of gray-scale levels which define a vesicle.

The behavior of vesicles observed in neurites of PC12 cells may help to clarify the mechanical task (forces required, energy efficiency) faced by motor proteins in neurons. Failure to accomplish this mechanical task could play a role in neurodegenerative disease (Goldstein 2001; Goldstein and Yang 2000; Smith et al. 2001; Suomalainen et al. 1999; Welte et al. 1998).

Materials and methods

Cells

PC12 cells were obtained from the ATCC and grown largely following Greene's procedures (Greene et al.

1998). Cells were maintained as adherent cultures at 37 °C under 7.5% CO₂ in uncoated Becton-Dickinson T75 plastic flasks. The growth medium was high-glucose DMEM supplemented with 25 mM HEPES, 6% fetal bovine serum, 6% horse serum, 2 mM L-glutamine, and 50 units/mL penicillin-streptomycin (Life Technologies), pH 7.2. Cultures were subdivided every 3–5 days; the passage number was kept at 20 or less. To induce neurite formation, 1E5 cells were plated onto previously cleaned cover glasses coated with poly-L-lysine (Sigma), and the medium was changed to DMEM supplemented with 25 mM HEPES, 0.5% horse serum, 0.5% fetal bovine serum and 50 ng/mL NGF, pH 7.2. In this medium, cells established 100–200 µm long neurites in 3–7 days. For observation in the microscope, a cover glass with adherent cells on its upper surface was transferred to an open chamber containing the differentiation medium maintained at 35 °C. The cells remained alive for 1–2 h in this chamber and did not retract neurites.

Microscopy and image processing

The chamber was placed on the stage of a Nikon E600FN microscope equipped with 60× water immersion objective (NA 1.0, wd 2 mm) and DIC optics. A cooled 1.35 Mpixel progressive-scan CCD camera (Hamamatsu C6489) was used to digitize the images to a precision of 12 bits at 8.3 frames/s. To maximize the signal-to-noise ratio of images, the DIC phase offset (polarizer angle in the deSenarmont method) was set to the smallest value permitted by the phase shifts in the sample (Holzwarth et al. 2000). Source intensity was then adjusted to fill the camera's intensity range. A 12-bit background image was subtracted continuously from the incoming image stream by an image-processing board (Matrox Genesis, 64 MB) in a personal computer with 1 GB RAM. This made full use of the 4096 gray levels provided by the camera. Bits 10 to 3 or 9 to 2 of the background-subtracted image were normally selected for further 8-bit processing; bits 12 and 11 were usually empty because of the background-subtraction operation. Following contrast enhancement through a look-up table with adjustable slope, the background-subtracted images were displayed on an Image Systems M17L grayscale monitor. The overall processing time lag was 1 frame.

A 128-image sequence of the most recently processed images was continuously updated in a 400 Mb subsection of host RAM. Whenever a noteworthy event was observed, the most recent 128 images in host RAM were sent to a 19 GB hard drive, and ultimately to a CD, for long-term storage. Stored images were 512×512 pixel², or 55×55 µm².

Background images were constructed and continuously updated on the Matrox board during image acquisition by time-averaging the last 32 images and applying a 3×3 Sobel spatial smoothing filter to the result.

Vesicle tracking

Tracking was carried out by post-processing the background-subtracted images. The post-processing program was built around the family of pattern recognition functions of the image processing board. First, a pattern P was defined in the first image by a 10×10 or 12×12 (pixel)² area-of-interest with the selected vesicle at its center. Vesicle position in subsequent images I was determined by maximizing the normalized gray-scale cross-correlation:

$$\frac{N\Sigma(IP) - (\Sigma I)(\Sigma P)}{\sqrt{(N\Sigma I^2 - (\Sigma I)^2)(N\Sigma P^2 - (\Sigma P)^2)}} \quad (1)$$

between P and I . The summations are over the N pixels in the pattern. Unlike simple cross-correlation, this expression has low sensitivity to the mean intensity levels within P and I . The program computed the location of the maximum in the normalized cross-correlation to sub-pixel precision by interpolation. No assumptions are made about the analytic form of the image of a vesicle.

Vesicle radius was determined from a DIC image of the vesicle. We measured the distance between the minimum and the maximum in a line scan of the image along the sheer direction of the microscope. This method was tested using latex beads of known size (Interfacial Dynamics). The bead radii claimed by the manufacturer and the radii we determined (mean ± standard deviation, in µm) were (0.60; 0.60 ± 0.03), (0.55; 0.55 ± 0.03), (0.41; 0.41 ± 0.03), (0.29; 0.29 ± 0.03), (0.21; 0.21 ± 0.02), (0.11; 0.18 ± 0.03). The method works well for vesicles of radius 0.20 µm or greater. For smaller vesicles, the DIC image is enlarged by diffraction, so that such vesicles appear to have a radius of 0.20 µm.

A rectangular area 0.4 µm×0.4 µm enclosing a particle of radius 0.2 µm contains 16 pixels in our system.

Results

Vesicle movement

Vesicles of radius 0.25–0.5 µm could be discerned in unenhanced DIC images of live PC12 neurites, but their visibility was poor (Fig. 2, top). After background subtraction and aggressive contrast enhancement, the vesicles stood out clearly (Fig. 2, bottom). These image-processing operations were carried out in “real time” by a fast image-processing board. As a result, the rapid movement of vesicles along the neurite was apparent during experiments (Fig. 3). Because DIC microscopy with 546 nm light does not significantly damage live cells, traffic within a single neurite could be observed continuously for more than one hour. The visually observed vesicle flux through a cross-section of the neurite was approximately 0.5 vesicles/second, evenly divided between anterograde and retrograde motion. Out of all

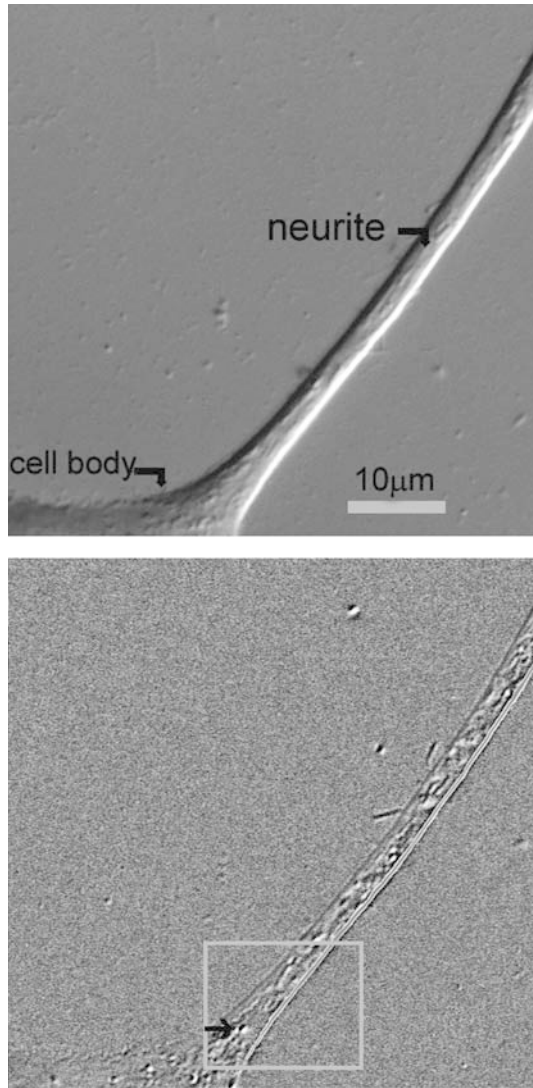


Fig. 2 Unstained PC12 cell after 4 days of NGF treatment. *Top*: DIC image of a typical neurite. The cell body is located in the *lower left corner*. *Bottom*: background-subtracted DIC image of the same neurite. The *arrow* indicates a vesicle and the *light-colored rectangle* defines an area of interest (AOI). Both images are 512×512 pixels. The AOI in the lower image is 150×120 pixel²

visible vesicles, approximately one in ten had sufficient contrast to be tracked. Vesicles were tracked to a precision of ± 30 nm by a pattern-matching algorithm described in Materials and methods.

Vesicles moved parallel to the neurite axis; no motion perpendicular to the axis was detected, within our precision limits. The net displacement $S(t)$ of a vesicle was calculated by summing the incremental distances,

$ds_i = \sqrt{(x_{i+1} - x_i)^2 + (y_{i+1} - y_i)^2}$, traversed between frames. A total of 57 vesicles in nine different cells were tracked offline for 50–128 frames (6–15 s). Visual inspection of plots of displacement against time suggested that individual vesicles traveled at a constant speed for 0.5–2 s, then abruptly changed to a different, but again constant, speed.

Model-free analysis

To obtain a model-free measure of the persistence of vesicle velocity, we computed the Fourier transform of the velocity of individual vesicles from a three-point slope:

$$v_i(t) = \frac{(r_i - r_{i-1}) + (r_{i+1} - r_i)}{t_{i+1} - t_{i-1}} \quad (2)$$

For comparison, the Fourier transform of the same set of velocities, but randomized in order, was also computed. Both transforms are shown in Fig. 4. The transform of the velocity of individual beads exceeds the transform for the randomized velocities for $0 \leq \omega \leq 8$ rad/s, but is below the random curve for higher frequencies. This suggests that the vesicle velocity persists for about $2\pi/8 = 0.8$ s. Alternatively, the transformed data for individual vesicles were fitted to a Lorentzian function:

$$L(\omega) = \frac{1}{\pi} \frac{\Gamma/2}{(\omega - \omega_0)^2 + (\Gamma/2)^2} \quad (3)$$

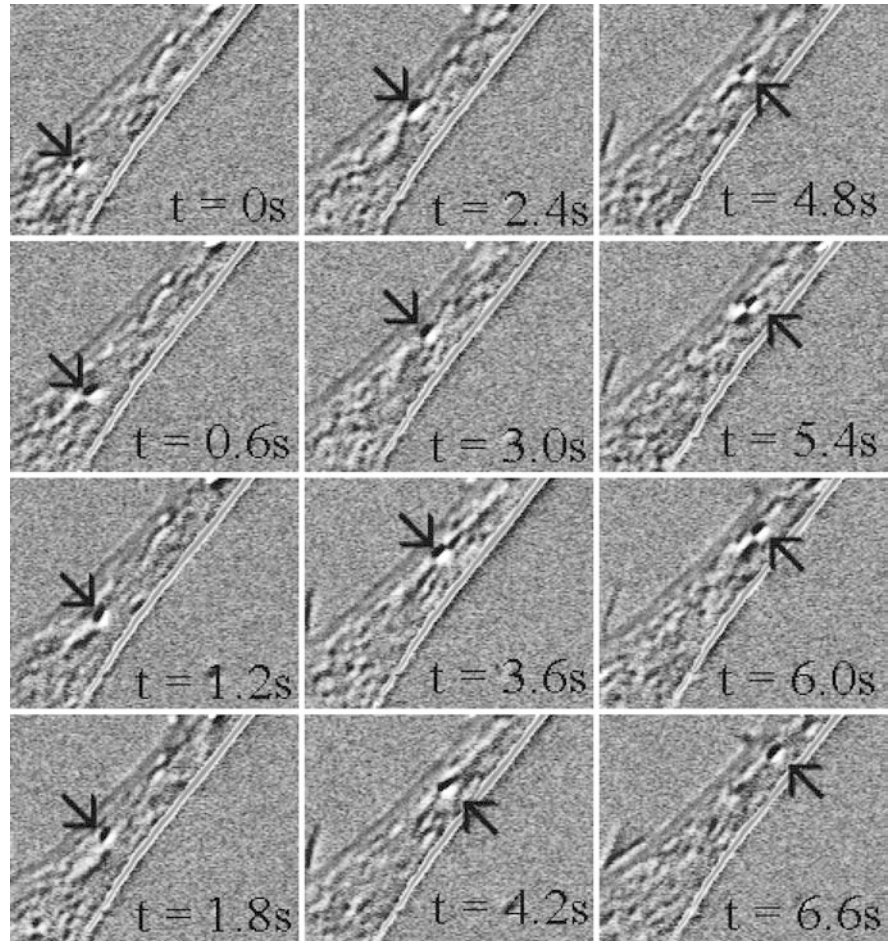
with $\omega_0 = 0$. Although the fit was not good, the best fit occurred with $\Gamma = 11.3 \text{ s}^{-1}$.

An alternative model-free measure of the persistence of velocity is to compute the autocorrelation of the velocity at time t with the velocity at time $t + \tau$. When the autocorrelation of single vesicles was computed and compared to a randomized data set, it was found to exceed the autocorrelation of the randomized data for $0 < \tau < 0.7$ s. For $\tau > 0.7$ s, the single-vesicle autocorrelation was indistinguishable from that of a randomized data set (data not shown).

Model with straight-line (constant-velocity) segments

Because such behavior could have mechanistic significance, we sought a more incisive way to analyze the vesicle tracks. We found that modeling the displacement of individual vesicles by a connected series of constant-velocity segments of variable duration fitted the data. Models with 2, 3, 4, ... 12 segments were tested. The 4–24 parameters, 2 per segment, were in each case adjusted to minimize the squared error between observed position data and the model, using the non-linear, constrained, least-squares minimization algorithm `fmincon` in Matlab. The reduced mean-squared error, χ_r^2 (Bevington 1969; Press et al. 2002), was computed for each optimized model, with the experimental uncertainty σ of individual vesicle position measurements set to 30 nm. This is the smallest observed variance of vesicle path from a straight line over 10 or more images in our tracking data. A value of χ_r^2 near 1.0 is the hallmark of a model which is statistically meaningful. We found that almost every vesicle track (3–15 s) had several periods of constant-velocity motion with local $\chi_r^2 \approx 1$, interspersed

Fig. 3 Image time-series showing vesicle movement within the AOI of Fig. 2. The frame rate was 8.3 s^{-1} ; every fifth image is shown. The data shown are a subset of data collected over longer durations



with periods of non-constant velocity for which χ_r^2 was larger.

To determine the optimum number of segments for a given vesicle track, the overall value of χ_r^2 was determined for $N_{\text{seg}} = 2-12$. The model with the smallest value of χ_r^2 was used for further analysis of that vesicle's motion. Figure 5 shows a measured track for a particular vesicle,

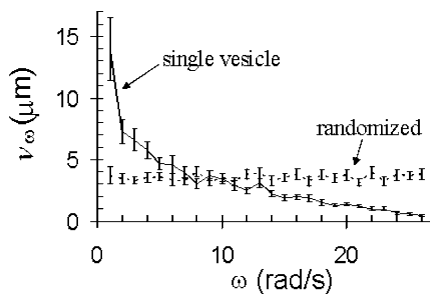


Fig. 4 Fourier transform of the velocity of vesicles in PC12. The solid line shows the result if the transform of the three-point velocity of individual vesicles was computed, then averaged for 59 vesicles. The dashed line shows the result, which is essentially “white”, after randomizing the three-point velocities in time, then computing the Fourier transform. The randomization was performed 30 times and the resultant transforms averaged. The error bars are standard deviations

together with its optimized model. The overall value of χ_r^2 was 1.16 for $N_{\text{seg}} = 7$; optimized models with a larger or smaller number of segments had larger values (Fig. 5, inset). Individual segments of the 7-segment model for this vesicle had values between 0.79 and 1.37. The value of χ_r^2 for 20 different vesicles was 3.7 ± 2.7 (mean \pm standard deviation). Most segments for the track of a given vesicle had values between 0.7 and 1.5, but about one-quarter of the segments had significantly higher χ_r^2 . This increased the overall χ_r^2 for the track of a given vesicle. For further analysis, the velocity of a vesicle at a particular moment was taken as the slope of the best-fit line-segment model at that time. This velocity must depend on the magnitude and direction of the driving forces and the velocity-dependent drag force on that vesicle.

Histogram of scaled velocities

To reduce the complicating effect of vesicle radius, we scaled the velocities of individual vesicles by v_0 , the minimum sustained speed for that vesicle. As expected for a range of vesicle sizes, v_0 had a broad distribution: $v_0 = 0.44 \pm 0.09 \text{ } \mu\text{m/s}$ (mean \pm standard deviation). The results of the velocity analysis are summarized in Fig. 6, which contains two histograms and an analysis of their

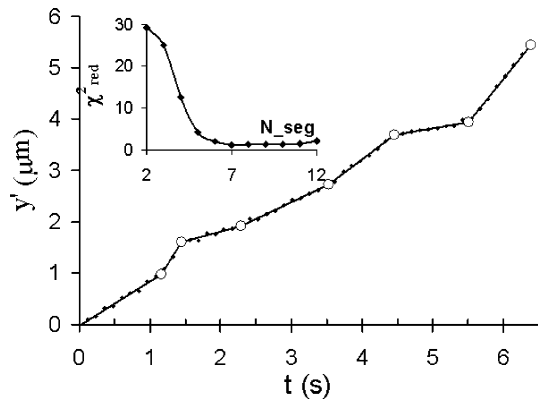


Fig. 5 Example of data showing the position of a vesicle in a neurite as a function of time, and the method used to determine the velocity. *Solid diamonds*: observed vesicle position. *Lines between open circles*: straight-line segments fitted to the data by least-squares optimization (MatLab Optimization Toolbox). The *inset* shows χ^2_{red} for N_{seg} between 2 and 12. The optimum value of N_{seg} was 7. This is the fit shown in the main part of the figure. The velocity of the vesicle was taken from the slope of the fitted curve

statistical significance. The single-vesicle histogram in Fig. 6A gives the frequency of occurrence of the scaled velocity v/v_0 for anterograde motion of individual vesicles. This histogram shows peaks at 2, 3, and 4 and a pronounced valley between 1 and 2.

To determine whether these features were statistically significant, we catenated all 59 single-vesicle datasets of measured velocities into a single superset of 2420 velocities, randomized the order of the elements in the superset, and then recut the superset into 59 smaller subsets corresponding to “randomized vesicles”. This procedure removed any relationship which might exist between the velocities of a single vesicle at different times, while keeping invariant the underlying experimental velocity dataset. The velocities of each randomized vesicle were then scaled by v_0 for that vesicle, just as for the real data. A histogram of v/v_0 for the “randomized vesicles” is shown as the randomized histogram in Fig. 6A. Unlike the histogram for real single-vesicle data, the histogram for the randomized data decreased monotonically with increasing v/v_0 .

To test the statistical significance of the differences between the two histograms in Fig. 6A, the normal deviate Z_i was computed for each bin i of the two histograms (Cox et al. 1988). For a Poisson distribution, Z_i is approximately normally distributed with a mean of zero and variance of one. Values of Z_i greater than 2 or less than -2 are generally considered statistically significant (Cox et al. 1988). A plot of Z_i against v/v_0 is shown in Fig. 6B. The Z -plot shows that the single-vesicle histogram differs significantly from the histogram of the randomized velocities. Notably, there are statistically significant positive peaks at 2, 3, and 4 and a significant negative valley between 1 and 2. Possible reasons for this non-random pattern within the single-vesicle histogram are explored in the Discussion.

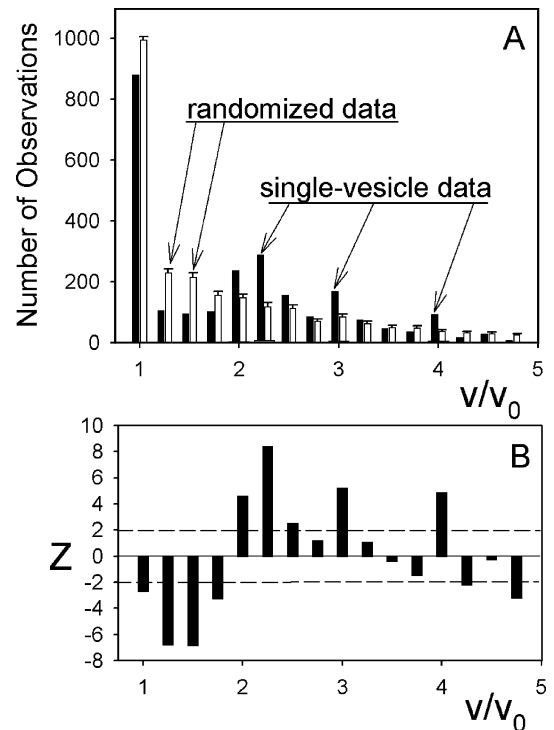


Fig. 6A, B Histograms of the scaled velocity v/v_0 . **A** shows a histogram of the reduced velocity v/v_0 for single vesicles (*black bars*) and a second histogram for randomized data (*white bars*). The procedure used to randomize the velocity data is described in the text. **B** is a channel-by-channel comparison of the normal deviate Z_i between the two histograms. For frequencies n_{1i} and n_{2i} in bin i , and the total number of observations n_1 and n_2 , the normal deviate was computed as $Z_i = (p_{1i} - p_{2i}) / \left[\frac{p_{1i}}{n_1} + \frac{p_{2i}}{n_2} \right]^{1/2}$, where $p_{1i} = \frac{n_{1i}}{n_1}$ and $p_{2i} = \frac{n_{2i}}{n_2}$. Normal deviate values greater than 2 or less than -2 are considered significant (Cox et al. 1988)

The average speed of vesicles in PC12 was $1.25 \pm 0.8 \mu\text{m/s}$ (59 vesicles, 2454 frames) in the anterograde direction. An additional 40 vesicles moving in the retrograde direction had an average speed of $1.2 \pm 0.7 \mu\text{m/s}$. These velocities are 35% greater than previously measured for secretory vesicles in PC12 neurites, $0.92 \mu\text{m/s}$ (Lochner et al. 1998). The average distance traveled by a vesicle before changing speed, \bar{L} , was $1.3 \mu\text{m}$ for both retrograde and anterograde movement. It has not escaped our notice that single kinesin motors travel a similar average distance, $1.4 \mu\text{m}$, before falling off a microtubule during bead assays (Block et al. 1990).

Brownian motion

To assess the drag force and work required to transport vesicles in PC12 neurites at the velocities we observe, we also determined the viscoelasticity of the medium in which the vesicles move. The viscoelasticity was deduced from careful measurements of the

Brownian motion of vesicles in live PC12 cells at 35–37 °C, the same temperature used for the fast transport measurements. We would have preferred to measure the Brownian motion of vesicles within the neurites. However, vesicles in neurites either moved in one direction parallel to the neurite axis, or they were stationary. Brownian motion was instead measured on 21 vesicles located immediately adjacent to the neurite but within the growth cones.

From the tracks of Brownian motion, we determined the squared displacement Δr^2 as a function of the time interval τ between observations (Fig. 7) over slightly more than 2 decades. The complex viscoelastic modulus $G^*(\omega)$ was found from these data by Mason's generalized Stokes–Einstein method (Mason 2000):

$$G^*(\omega) = \frac{k_B T}{a \Delta r^2 \Gamma(\alpha + 1)} \quad (4)$$

where Δr^2 is the squared displacement at $\tau = 1/\omega$, k_B is Boltzmann's constant, T is the absolute temperature, a is the vesicle radius, Γ is the Gamma function, and α is the slope of a log-log plot of Δr^2 as a function of τ . The value of α varied between 0.7 and 0.8 for τ between 0.12 s and 5.6 s. For longer values of τ , where the statistical uncertainties of our data are largest, α increased sharply, becoming unphysical ($\alpha > 1$). We therefore used a polynomial fit to the data between 0.12 s and 5.6 s to determine α over the range $0.12 < \tau < 15$ s. The resultant ratio of the real to the imaginary parts of the complex viscoelastic modulus, G'/G'' , was approximately 0.5 over the whole range of ω . Slopes of log-log plots of the storage modulus $G'(\omega)$ and loss modulus $G''(\omega)$ versus ω were both 0.8 (data not shown), although the large uncertainties in the primary data (Fig. 7) make this value approximate.

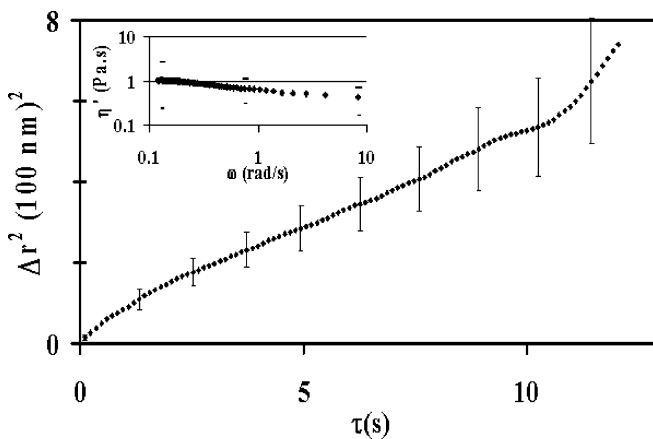


Fig. 7 Brownian motion of vesicles within the growth cones but proximal to the neurites of PC12 cells, at 35 °C, plotted as Δr^2 versus τ . The values of Δr^2 are an average for 21 vesicles. The large error bars arise because Brownian motion is a random process. The average vesicle radius was 0.23 μm , with a range of 0.20–0.35 μm . *Inset:* the viscosity $\eta(\omega)$ for PC12 cytoplasm, as determined from the Brownian motion by the generalized Stokes–Einstein method. Error bars are indicated at three values of ω . The limiting viscosity at low frequency is 1.1 Pa s

The frequency-dependent viscosity, $\eta'(\omega)$, was determined from $G^*(\omega)$:

$$\eta' = \frac{G''}{\omega} \quad (5)$$

where G'' is the imaginary part of $G^*(\omega)$. The viscosity $\eta'(\omega)$ of PC12 cytoplasm was found to be shear-thinning, as expected for a fluid rich in polymers, but reached a plateau at small ω (Fig. 7, insert). The zero-frequency viscosity of PC12 cytoplasm was 1.1 ± 0.25 Pa s at 35–37 °C for vesicles with a radius of 0.20–0.35 μm . This is 1500 times the viscosity of the buffer in bead assays, but 50-fold less than the viscosity measured from the Brownian motion of fat globules in COS7 cells (Yamada et al. 2000). We tested our implementation of Mason's GSE method with beads of known size in water, and recovered the known viscosity of water and its Newtonian behavior (Hill 2003).

Once $\eta'(\omega)$ was known, the drag force on vesicles undergoing fast transport in neurites was calculated from Stokes' law:

$$F = 6\pi\eta a v \quad (6)$$

where η is the zero-frequency viscosity, v is the vesicle velocity, and a is the vesicle radius. This procedure is justified here even though the medium is viscoelastic (Holzwarth et al. 2002). The measured velocities and the required drag forces (from Stokes' law) for four typical anterograde vesicles during three consecutive periods of constant velocity are given in Table 1.

Discussion

The results in Figs. 4, 5, and 6 show that individual vesicles of radius 0.30–0.45 μm move along a neurite in PC12 cells in a series of constant-velocity segments lasting 1–2 s. If one takes a global view of the velocities of many vesicles, a broad, featureless distribution is obtained (Hill 2003). However, if one takes a “single vesicle” viewpoint and reduces the velocities by the smallest velocity of that vesicle, one finds that the distribution of the reduced velocity has statistically significant peaks near 2, 3, and 4 and a statistically

Table 1 Velocities and forces on vesicles^a

Vesicle	Radius (μm)	Velocity ($\mu\text{m/s}$)			Force (pN)		
		V_1	V_2	V_3	F_1	F_2	F_3
1	0.35	1.72	0.58	1.28	12.3	4.1	9.1
2	0.40	0.94	0.45	1.14	7.7	3.7	9.3
3	0.35	1.47	0.65	1.37	10.5	4.6	9.8
4	0.35	0.99	0.59	2.02	7.1	4.2	14.4

^aThe lowest force, which happens in this case to have occurred during the middle segment, varied between 3.7 and 4.6 pN. The maximum force was 14.4 pN

significant absence of reduced velocities between 1 and 2 (Fig. 6).

In our view, three of the more likely sources of this behavior are:

1. The number of *motors* actively pulling a vesicle may change between 1, 2, 3, and 4 at various times.
2. Each vesicle may have many motors bound to its surface, but the number of *microtubules* sufficiently close to the vesicle may change from 1 to 2 to 3 as the vesicle moves along the neurite.
3. The viscosity may vary in different parts of the neurite.

The first explanation is favored by several arguments. First, it is likely that anterograde transport in PC12 neurites is driven by members of the kinesin family, because the MTs in PC12 neurites are oriented with their plus-ends distal, as in axons (Okabe and Hirokawa 1988), and kinesins are the primary plus-end-directed motors in neurons. The maximum force exerted by conventional kinesin in bead assays is 6.5–7.5 pN (Nishiyama et al. 2001; Visscher et al. 1999), about twice what is needed to move a vesicle at v_0 in PC12 (Table 1). Electron micrographs show that transported mitochondria in *Reticulomyxa* filaments carry only a small number (1–4) of motors (Ashkin et al. 1990).

Second, when we examined the positions at which different vesicles moving along the same track change speeds within a given neurite, only a loose correlation was found (Hill 2003). This indicates that changes in the speeds of vesicles are probably not caused by “switch-yards” in the MT railway system or by spatial variations in viscosity. Moreover, the constant-velocity segments had a characteristic length of 1.3 μm for both retrograde and anterograde motion, in good agreement with the average run length, 1.4 μm , reported for a single kinesin attached to a bead moving in buffer against no trapping force (Block et al. 1990). This result supports the view that vesicles change speed whenever the number of active motors changes.

The forces exerted by motor proteins within cells have previously been measured in two systems. In *Reticulomyxa*, optical trap manipulations show that the maximum force generated by a single motor is 2.6 pN (Ashkin et al. 1990). Within *Drosophila* embryos, the stall forces on lipid droplets during different developmental phases are 1.1, 3.3, 4.7, and 5.5 pN (Welte et al. 1998). The presumed single-motor stall force in *Drosophila* is thus 1.1 pN. These data suggest that the steplike velocity changes observed in PC12 vesicles could arise from changes in the number of motors. Previous studies of the transport of lipid droplets in *Drosophila* embryos (Gross et al. 2000; Gross et al. 2002) have noted that these droplets often backtrack. This was not generally observed for vesicles in PC12 neurites. Only three vesicles exhibited backtracking, and then for only 0.5 s out of a 15 s data set.

For this reason, backtracking was excluded from the analysis. Vesicles moving with $v < 0.20 \mu\text{m/s}$ were also excluded from consideration since their velocity was too slow to be classified as fast axonal transport.

It is sometimes argued, incorrectly, that changing the number of motors should not affect the velocity of a vesicle if the motors are kinesins, because kinesin is processive. This view originates from early kinesin gliding assays in buffer, which showed that the velocity is constant over a broad range of kinesin surface density (Howard et al. 1989). However, as discussed in the Introduction, the load in these early gliding assays was less than 0.1 pN, because the medium was buffer (Gibbons et al. 2001). Gliding assays in a more viscous medium give an entirely different picture: the velocity decreases with increasing load at low kinesin densities yet remains constant at high kinesin densities (Hunt et al. 1994). This is what Fig. 1 predicts. Fast transport of large vesicles in PC12 cells requires a force of 4–15 pN (Table 1). In this force range, the number of motors does matter (Fig. 1). The fact that kinesin is processive does not change this argument.

We should point out that the Stokes’ law curve in Fig. 1 predicts that vesicle velocity should be sublinear in the number of motors, but Fig. 6 suggests a linear relation. However, Fig. 1 is only semi-quantitative, because the data used to construct the curves for 1, 2, and 3 motors in the figure were derived from single-motor bead assays in calibrated optical traps. The maximum average bead velocity, v_{max} , at zero load is only 800 nm/s in such trap experiments. Corresponding force–velocity curves for cells, which would be more appropriate, have not yet been determined. However, the maximum velocity of vesicles in neurons is roughly 3500–5000 nm/s (Brady et al. 1982; Grafstein and Forman 1980; Kaether et al. 2000) This five-fold increase in v_{max} in cells, which occurs despite a large increase in viscosity, could explain the apparent inconsistency between Figs. 1 and 6. An F – v curve that properly accounted for the observed velocities of vesicles in cells would make the Stokes’ law prediction more nearly linear in the number of motors.

The average vesicle anterograde velocity we observed in PC12 neurites, 1.25 $\mu\text{m/s}$, is higher than the average velocity previously reported for fluorescently labeled secretory vesicles in PC12, 0.92 $\mu\text{m/s}$ (Lochner et al. 1998). Our velocities are within the range, 0.8–4 $\mu\text{m/s}$, which defines fast axonal transport (Howard 2001). We estimate that we are able to track about 10% (by number) of the total vesicle traffic visible by background-subtracted DIC. The contrast of the remaining vesicles was too low for reliable optical tracking by our current methods. The average velocity of retrograde vesicles was 1.15 $\mu\text{m/s}$. However, fewer retrograde vesicles could be tracked, weakening statistical arguments. A histogram of their scaled velocities did not show the same pattern as anterograde vesicles (Hill, 2003).

By GFP labeling of UNC-104 within *C. elegans*, Scholey and co-workers have directly observed the movement of a motor in a cell (Zhou et al. 2001). The average velocity of the motor was 1.0 $\mu\text{m/s}$ but the peak velocity of individual fluorescent spots was 4.9 $\mu\text{m/s}$. The velocity of individual motors was constant for long distances, then changed abruptly to a different constant velocity (see Zhou et al. 2001, fig. 4B), much like our observations in PC12.

In conclusion, vesicles undergoing fast transport in PC12 neurites do not move in an all-or-none fashion. However, they do exhibit steplike changes in velocity. These velocity changes probably arise from changes in the number of active motor proteins attached to a particular vesicle at a particular time. The number of motors appears to vary between 1 and 5. A force of approximately 4 pN per motor is sufficient to propel the vesicles at the observed velocities.

Acknowledgements We thank Professors Carol Milligan and Dan Johnson, and Jason Newbern, for help with growth of PC12. We are grateful to Jennifer Shuler and Anita McCauley for guidance with immuno-labeling. We thank Hamamatsu Photonic Systems for the loan of a camera. Finally, we are grateful to Wake Forest University for support of this project through a Cross-Campus Collaboration Grant.

References

- Allen RD, Metzals J, Tasaki I, Brady ST, Gilbert SP (1982) Fast axonal transport in squid giant axon. *Science* 218:1127–1128
- Ashkin A, Schuetze K, Dziedzic JM, Euteneuer U, Schliwa M (1990) Force generation of organelle transport measured in vivo by an infrared laser trap. *Nature* 348:346–348
- Bevington PR (1969) Data reduction and error analysis for the physical sciences. McGraw-Hill, New York
- Block SM, Goldstein L, Schnapp BJ (1990) Bead movement by single kinesin molecules studied with optical tweezers. *Nature* 348:348–352
- Brady ST, Lasek RJ, Allen RD (1982) Fast axonal transport in extruded axoplasm from squid giant axon. *Science* 218:1129–1131
- Cox C, Reeder JE, Robinson RD, Suppes SB, Wheelless LL (1988) Comparison of frequency distributions in flow cytometry. *Cytometry* 9:291–298
- Freed JJ, Lebowitz MM (1970) The association of a class of saltatory movements with microtubules in cultured cells. *J Cell Biol* 45:334–354
- Gibbons F, Chauwin J-F, Desposito M, Jose JV (2001) A dynamic model of kinesin-microtubule motility assays. *Biophys J* 80:2515–2526
- Goldstein L (2001) Kinesin molecular motors: transport pathways, receptors, and human disease. *Proc Natl Acad Sci USA* 98:6999–7003
- Goldstein LSB, Yang Z (2000) Microtubule-based transport systems in neurons: the roles of kinesins and dyneins. *Annu Rev Neurosci* 23:39–71
- Grafstein B, Forman DS (1980) Intracellular transport in neurons. *Physiol Rev* 60:1167–1283
- Greene LA, Frinelli SE, Cunningham ME, Park DS (1998) Culture and experimental use of the PC12 rat pheochromocytoma cell line. In: Banker G, Goslin K (eds) *Culturing nerve cells*. MIT Press, Cambridge, pp 000–000
- Gross SP, Welte MA, Block SM, Wieschaus EF (2000) Dynein-mediated cargo transport in vivo: a switch controls travel distance. *J Cell Biol* 148:945–955
- Gross SP, Welte MA, Block SM, Wieschaus EF (2002) Coordination of opposite-polarity microtubule motors. *J Cell Biol* 156:715–724
- Hill DB (2003) Changes in the number of molecular motors driving vesicle transport in PC12. PhD thesis. Wake Forest University, Winston-Salem
- Hirokawa N (1998) Kinesin and dynein superfamily proteins and the mechanism of organelle transport. *Science* 279:519–526
- Holzwarth GM, Hill DB, McLaughlin EB (2000) Polarization-modulated differential interference contrast microscopy with a variable retarder. *Appl Opt* 39:6288–6294
- Holzwarth G, Bonin K, Hill DB (2002) Forces required of kinesin during processive transport through cytoplasm. *Biophys J* 82:1784–1790
- Howard J (2001) *Mechanics of motor proteins and the cytoskeleton*. Sinauer, Sunderland, Mass
- Howard J, Hudspeth AJ, Vale RD (1989) Movement of microtubules by single kinesin molecules. *Nature* 342:154–158
- Hunt AJ, Gittes F, Howard J (1994) The force exerted by a single kinesin molecule against a viscous load. *Biophys J* 67:766–781
- Kaether C, Skehel P, Dotti CG (2000) Axonal membrane proteins are transported in distinct carriers: a two-color video microscopy study in cultured hippocampal neurons. *Mol Biol Cell* 11:1213–1224
- Kojima H, Muto E, Higuchi H, Yanagida T (1997) Mechanics of single kinesin molecules measured by optical trapping nanometry. *Biophys J* 73:2012–2022
- Lochner JE, Kingma M, Kuhn S, Meliza CD, Cutler B, et al. (1998) Real-time imaging of the axonal transport of granules containing a tissue plasminogen activator/green fluorescent protein hybrid. *Mol Biol Cell* 9:2463–2476
- Mason TG (2000) Estimating the viscoelastic moduli of complex fluids using the generalized Stokes–Einstein equation. *Rheol Acta* 39:371–378
- Meyhoefer E, Howard J (1995) The force generated by a single kinesin molecule against an elastic load. *Proc Natl Acad Sci USA* 92:574–578
- Nishiyama M, Muto E, Inoue Y, Yanagida T, Higuchi H (2001) Substeps within the 8-nm step of the ATPase cycle of single kinesin molecules. *Nat Cell Biol* 3:425–428
- Okabe S, Hirokawa N (1988) Microtubule dynamics in nerve cells: analysis using microinjection of biotinylated tubulin into PC12 cells. *J Cell Biol* 107:651–664
- Press WH, Flannery BP, Teukolsky SA, Vetterling WT (2002) *Numerical recipes in C++: the art of scientific computing*. Cambridge University Press, Cambridge
- Rebuhn L (1967) Saltatory particle movements and their relation to the mitotic apparatus. In: Levine L (ed) *The cell in mitosis*. Academic Press, New York, pp 67–106
- Schliwa M (2003) *Molecular motors*. Wiley-VCH, Weinheim
- Schnitzer MJ, Visscher K, Block SM (2000) Force production by single-kinesin motors. *Nat Cell Biol* 2:718–723
- Smith GA, Gross SP, Enquist LW (2001) Herpes viruses use bidirectional fast-axonal transport to spread in sensory neurons. *Proc Natl Acad Sci USA* 98:3466–3470
- Suomalainen M, Nakano MY, Keller S, Boucke K, Stidwill UP, et al. (1999) Microtubule-dependent plus- and minus-end-directed motilities are competing processes for nuclear targeting of adenovirus. *J Cell Biol* 144:657–672
- Svoboda K, Schmidt CF, Schnapp BJ, Block SM (1993) Direct observation of kinesin stepping by optical trapping interferometry. *Nature* 365:721–727
- Vale RD, Funatsu T, Pierce DW, Romberg L, Harada Y, et al. (1996) Direct observation of single kinesin molecules moving along microtubules. *Nature* 380:451–453

- Visscher K, Schnitzer MJ, Block SM (1999) Single kinesin molecules studied with a molecular force clamp. *Nature* 400:184–189
- Welte MA, Gross S, Postner M, Block S, Wieschaus E (1998) Developmental regulation of vesicle transport in *Drosophila* embryos: forces and kinetics. *Cell* 92:547–557
- Yamada S, Wirtz D, Kuo SC (2000) Mechanics of living cells measured by laser tracking microrheology. *Biophys J* 78:1736–1747
- Zhou MH, Mascher IB, Scholey JM (2001) Direct visualization of the movement of the monomeric axonal transport motor UNC-104 along neuronal processes in living *Caenorhabditis elegans*. *J Neurosci* 21:3749–3755